Geochemistry, Geophysics, Geosystems®

AGU ADVANCING EARTH AND SPACE SCIENCES

RESEARCH ARTICLE
10.1029/2023GC010988

The Relation Between Decadal Droughts and Eruptions of Steamboat Geyser in Yellowstone National Park, USA

Shaul Hurwitz[1], John C. King[2], Gregory T. Pederson[3], Mara H. Reed[4], Lauren N. Harrison[1], Jefferson D. G. Hungerford[5], R. Greg Vaughan[6], and Michael Manga[4]

[1]Volcano Science Center, U.S. Geological Survey, Menlo Park, CA, USA, [2]Lone Pine Research, Bozeman, MT, USA, [3]Northern Rocky Mountain Science Center, U.S. Geological Survey, Bozeman, MT, USA, [4]University of California, Berkeley, Berkeley, CA, USA, [5]Yellowstone Center for Resources, Yellowstone National Park, WY, USA, [6]Astrogeology Science Center, U.S. Geological Survey, Flagstaff, AZ, USA

Abstract In the past century, most eruptions of Steamboat Geyser in Yellowstone National Park's Norris Geyser Basin were mainly clustered in three episodes: 1961–1969, 1982–1984, and ongoing since 2018. These eruptive episodes resulted in extensive disturbance to surrounding trees. To characterize tree response over time as an indicator of geyser activity adjustments to climate variability, aerial and ground images were analyzed to document changes in tree coverage around the geyser since 1954. Radiocarbon dating of silicified tree remnants from within 14 m of the geyser vent was used to examine geyser response to possible variations in decadal to centennial precipitation patterns. We searched for atypical or absent growth rings in cores from live trees in years associated with large geyser eruptions. Photographs indicate that active eruptive phases have adversely affected trees up to 30 m from the vent, primarily in the dominant downwind direction. Radiocarbon dates indicate that the geyser formed before 1878, in contrast to the birthdate reported in historical documents. Further, the ages of the silicified trees cluster within three episodes that are temporally correlated with periods of relative drought in the Yellowstone region during the 15th–17th centuries. The discontinuous growth of trees around the geyser suggests that changes in eruptive patterns occur in response to decadal to multidecadal droughts. This inference is supported by the lack of silicified specimens with more than 20 annual rings and by the existence of atypical or missing rings in live trees during periods of extended geyser activity.

Plain Language Summary Steamboat Geyser, in Yellowstone National Park's Norris Geyser Basin, has the tallest eruptions among the world's active geysers. To examine whether eruptions impact trees in the vicinity of the geyser, we analyzed aerial photos acquired since 1954 which indicate that prior periods of frequent eruptions have adversely affected trees up to 30 m from the vent, primarily in the dominant wind direction. To examine if the limited availability of water may have caused the geyser to stop erupting in past centuries, we dated silicified tree remnants with radiocarbon. Results suggest that trees were growing near Steamboat during three periods when the geyser was not erupting because of prolonged droughts in the Yellowstone region during the 15th–17th centuries. This inference is supported by observations that none of the silicified tree specimens had more than 20 annual rings, implying that the trees did not grow for long periods, and by the presence of atypical or missing rings in live trees during periods of geyser activity.

Key Points:

- Aerial photos indicate that recent eruptive phases of Steamboat Geyser have adversely impacted trees up to 30 m from the vent
- ^{14}C dates of silicified trees cluster in three periods that temporally correlate with regional droughts during the 15th–17th centuries
- Atypical or absent tree-rings suggest that prolonged eruption episodes impacted tree growth around Steamboat Geyser

Correspondence to:
S. Hurwitz,
shaulh@usgs.gov

Citation:
Hurwitz, S., King, J. C., Pederson, G. T., Reed, M. H., Harrison, L. N., Hungerford, J. D. G., et al. (2023). The relation between decadal droughts and eruptions of Steamboat Geyser in Yellowstone National Park, USA. *Geochemistry, Geophysics, Geosystems*, *24*, e2023GC010988. https://doi.org/10.1029/2023GC010988

Received 4 APR 2023
Accepted 8 JUN 2023

Author Contributions:
Conceptualization: Shaul Hurwitz, John C. King, Jefferson D. G. Hungerford, Michael Manga
Data curation: Shaul Hurwitz, John C. King
Formal analysis: Shaul Hurwitz, John C. King, Gregory T. Pederson, Mara H. Reed, Lauren N. Harrison
Funding acquisition: Michael Manga
Investigation: Shaul Hurwitz, John C. King, Gregory T. Pederson, Mara H. Reed, Lauren N. Harrison, Jefferson D. G. Hungerford

1. Introduction

The rarity of natural geysers reflects the special conditions needed for their formation: availability of water, a supply of heat, and a subsurface that has the right geometry of fractures and cavities to permit episodic discharge (Hurwitz & Manga, 2017). Decreased water supply to geysers in response to geothermal energy production (Barrick, 2007; White, 1992) or severe multidecadal regional droughts (Hurwitz et al., 2020) can lead to eruption cessation. Another mechanism to suppress geyser eruptions is by submerging the vent, for example, if landslides dam rivers and impound water (Kiryukhin, 2016). About half of the world's geysers are in Yellowstone National Park (USA), where much information on recent geyser activity has been documented (e.g., Hurwitz & Lowenstern, 2014; Hurwitz et al., 2014; Karlstrom et al., 2013; Kedar et al., 1998; Nayak et al., 2020; Reed et al., 2021; Vandemeulebrouck et al., 2014; Wu et al., 2019, 2021) and compiled by geyser enthusiasts (geysertimes.org). However, significantly less is known about geyser activity prior to the geologic expeditions in the second half of the 19th century when written documentation became available (e.g., Hayden, 1883; Peale, 1883; Whittlesey & Watry, 2008).

Methodology: Shaul Hurwitz, John C. King, Gregory T. Pederson, Mara H. Reed, Lauren N. Harrison, Jefferson D. G. Hungerford
Project Administration: Shaul Hurwitz, Jefferson D. G. Hungerford
Resources: Jefferson D. G. Hungerford
Software: Shaul Hurwitz, Gregory T. Pederson
Supervision: Shaul Hurwitz, Michael Manga
Visualization: Mara H. Reed, Lauren N. Harrison
Writing – original draft: Shaul Hurwitz
Writing – review & editing: John C. King, Gregory T. Pederson, Mara H. Reed, Lauren N. Harrison, Jefferson D. G. Hungerford, R. Greg Vaughan, Michael Manga

With the incorporation of continuous digital data sets in the past few decades, the response of the hydrothermal system in Yellowstone National Park to seasonal hydrologic cycles was well documented (Fournier et al., 2002; Gaspard et al., 2021; Hurwitz et al., 2007, 2008, 2010, 2014; Jaworowski et al., 2013). However, documenting changes in hydrothermal activity in response to climate variability at multi-decadal to centennial timescales requires accurate and precise dating of proxy materials for both hydrothermal activity and climate (Slagter et al., 2019). In Yellowstone National Park, studies that related changes in hydrothermal activity to climate variability mostly relied on radiocarbon (^{14}C) dating of organic material (e.g., Hurwitz et al., 2020; Morgan et al., 2022; Pierce et al., 2002; Schiller et al., 2020, 2022), but this method is challenging because significant non-atmospheric carbon can be circulating in the hydrothermal system (Churchill et al., 2020; Schiller et al., 2021). Radiocarbon dating of partly silicified wood preserved in the siliceous sinter mound of Old Faithful Geyser in Yellowstone National Park's Upper Geyser Basin (UGB) (Figure 1a) is an exception; there, ^{14}C dates were interpreted to indicate tree growth during severe multidecadal regional droughts in the 13th and 14th centuries, toward the end of the Medieval Climate Anomaly (Hurwitz et al., 2020).

The inference that Old Faithful Geyser was not erupting for about a century was based on observations that trees do not currently grow on, or near, the mounds of erupting geysers. Lodgepole pine tree remnants like those from Old Faithful Geyser can be preserved for many centuries (e.g., Hellawell et al., 2015; Hurwitz et al., 2020; Liesegang & Gee, 2020) because silica-rich alkaline thermal waters erupted by the geyser deposit amorphous silica that prevents the disintegration of cellulose by fungi, bacteria, and insects (Blanchette, 1995). Conversely, in Yellowstone National Park's nonthermal areas, lodgepole pine deadwood seldomly exceeds 300 years old (Despain, 1983).

In March 2018, after 34 years of infrequent, sporadic activity, Steamboat Geyser in Yellowstone National Park's Norris Geyser Basin (NGB) (Figure 1) began a prolific sequence of eruptions. The reason for the geyser's reactivation remains uncertain, but eruption intervals between 2018 and 2020 (3–35 days) were slightly modulated seasonally, which may suggest a relation between the annual hydrological cycle and the geyser's eruptions (Reed et al., 2021). Further, because active geysers require a continuous supply of large amounts of water, periods of activity and dormancy could be affected by changing climate (Hurwitz & Manga, 2017). Dr. A.C. Peale, a member of the 1878 Hayden survey wrote about Steamboat Geyser "*Trees standing in the line of this sand-flood are dead, and a number uprooted and covered with sand, and some of the trees back of the vents have had their foliage killed, but it had not yet fallen from them. Everything seems to point to the fact of the recent formation of the vent*." Dr. Peale then writes, "*Mr. Norris informs me that in 1875 the vent had no existence, and in his report for 1879 he gives the date of its formation as 11 August 1878*" (Hayden, 1883, pp. 128–129). Based on available records, Steamboat Geyser's recorded eruption intervals have ranged from 3 days to 50 years and mostly clustered in three episodes: September 1961–early 1969, January 1982–September 1984, and ongoing since March 2018 (Reed et al., 2021).

To quantify how trees respond to geyser eruptions, we first analyze aerial imagery to document changes in the forest surrounding Steamboat Geyser since 1954, the first year from when aerial images are available. We then test the assertion that Steamboat Geyser formed in 1878 and examine geyser response to decadal anomalies in Yellowstone River streamflow and Norris Basin snowpack. Annual streamflow integrates the influence of temperature, precipitation, and evapotranspiration on surface and groundwater hydrology, whereas snowpack is primarily representative of cool-season total precipitation and temperature (Martin et al., 2020; Pederson et al., 2011, 2013). For this assessment, we collected 20 specimens of partly silicified wood from tree remnants that grew at distances of less than 14 m from the geyser vent for ^{14}C dating. We also collected cores from live trees surrounding the geyser's active sinter mound to search for atypical or absent rings during years associated with recent large geyser eruptions. We a priori assume that changes in geyser eruptive activity can cause discontinuous growth of proximal trees, with trees growing undisturbed during periods of geyser inactivity (Hurwitz et al., 2020). We then compare the ^{14}C dates of the tree remnants with regional hydroclimate indices (Martin et al., 2019a, 2019b, 2020) to examine if there is a temporal correlation between Steamboat Geyser eruptions and climate variability at the decadal to centennial timescales.

2. Steamboat Geyser

Steamboat Geyser, considered to have the tallest eruptive plume (~115 m; White et al., 1988) among the world's active geysers, is in Yellowstone National Park's NGB (Figure 1), just outside the northern rim of the Yellowstone caldera. The bedrock in NGB consists of the Lava Creek Tuff (White et al., 1988), which erupted when the 0.631-Ma Yellowstone caldera was formed (Christiansen, 2001; Matthews et al., 2015). Throughout most of the basin, the Lava Creek Tuff is covered by siliceous sinter, glacial, alluvial, and lacustrine deposits. Present-day

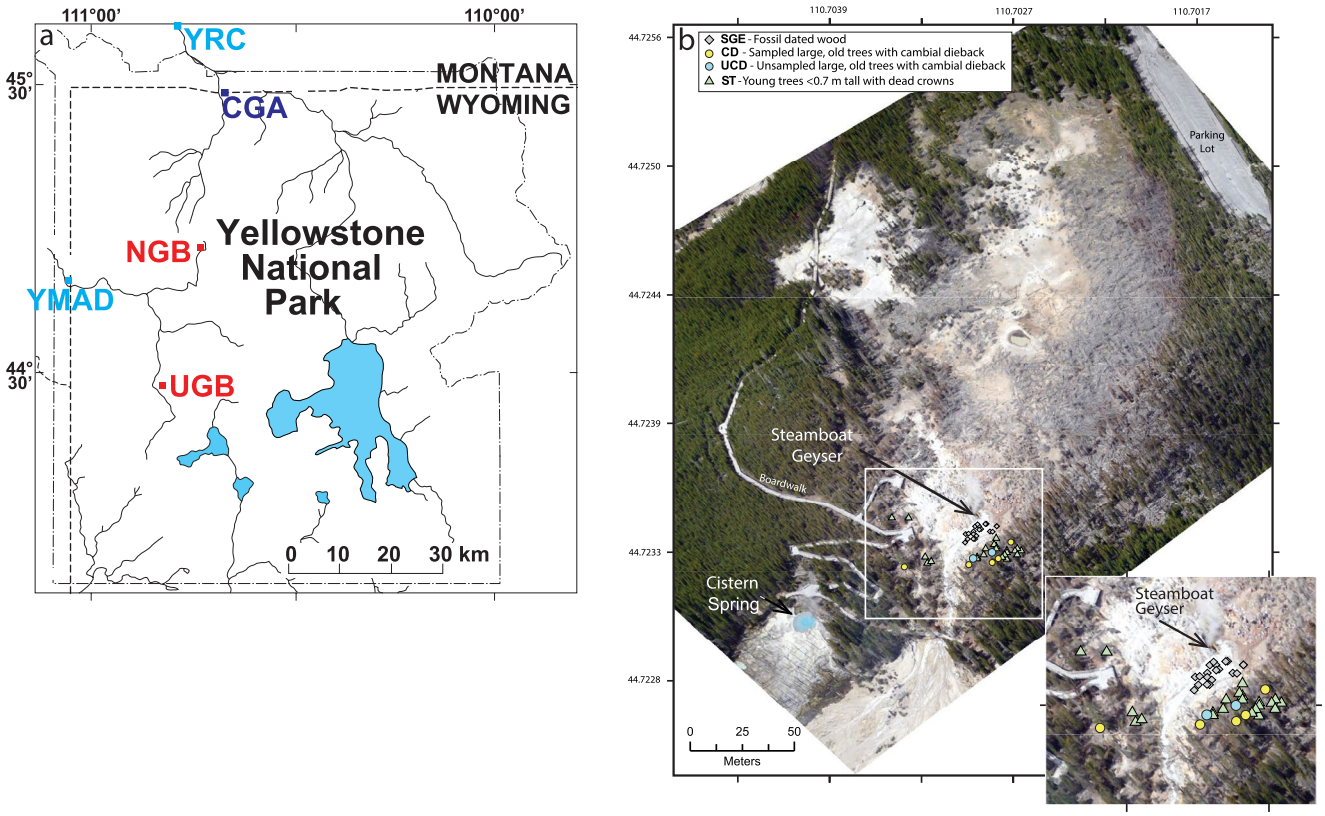

Figure 1. (a) Map of Yellowstone National Park showing the locations of Norris Geyser Basin, the Upper Geyser Basin, the gage on the Yellowstone River at Corwin Springs, Montana (YCR; USGS 6191500; U.S. Geological Survey, 2022), and the Chinese Garden Expanded tree chronology area (CGA) from which the hydroclimate record used in this study was reconstructed (King, 2016). Madison River near West Yellowstone, Montana is the gage on the Madison River near West Yellowstone (USGS 06037500; U.S. Geological Survey, 2022) (b) Aerial photo of the Steamboat Geyser area taken on 16 May 2020 showing in the inset the locations where samples were collected. Photo by Janet Jones.

Steamboat Geyser consists of two vents in an open hillside strewn with boulders and rock fragments (Figure 1b). Thin sinter deposits exist in and around the vents and along the geyser's major runoff channels; the rest of the exposed rock is altered Lava Creek Tuff (White et al., 1988).

Minor eruptions at Steamboat Geyser typically have vertical jets of up to 15 m from one or both vents. Major eruptions at Steamboat Geyser over the past century were mainly clustered in three time periods (Figure 2): (a) between early September 1961 and early 1969, (b) between 13 January 1982 and 26 September 1984, and (c) since 15 March 2018 with decreasing frequency in 2022. Major eruptions begin like minor eruptions but become progressively taller with a liquid phase that lasts for 3–90 min and a steam phase that slowly diminishes over many hours (Reed et al., 2021). Some major eruptions in the 1960s reached maximum heights of 83–116 m, based on triangulation from photographs (Gastellum, 1963; Schroeder, 1963). Following the end of the final steam phase, Steamboat Geyser discharges no water until minor eruptions resume several days later. The geyser's powerful eruptions have prevented tree growth up to 30 m from the vent.

It was initially proposed that the sequence of Steamboat Geyser eruptions that commenced in 2018 was a manifestation of uplift episodes centered near NGB between late 2013 and March 2014 and between 2016 and at least through the end of 2018. The uplift episodes were interpreted as shallowing of magma-derived volatile accumulation in the upper crust (Wicks et al., 2020). However, no changes in the subsurface reservoir temperature across this period were found (Reed et al., 2021).

3. Analysis of Aerial Photos

Aerial photography has been conducted in Yellowstone National Park at irregular intervals and varied spatial resolutions since 1954 (Shean, 2006). We searched for images of NGB acquired around the time of Steamboat

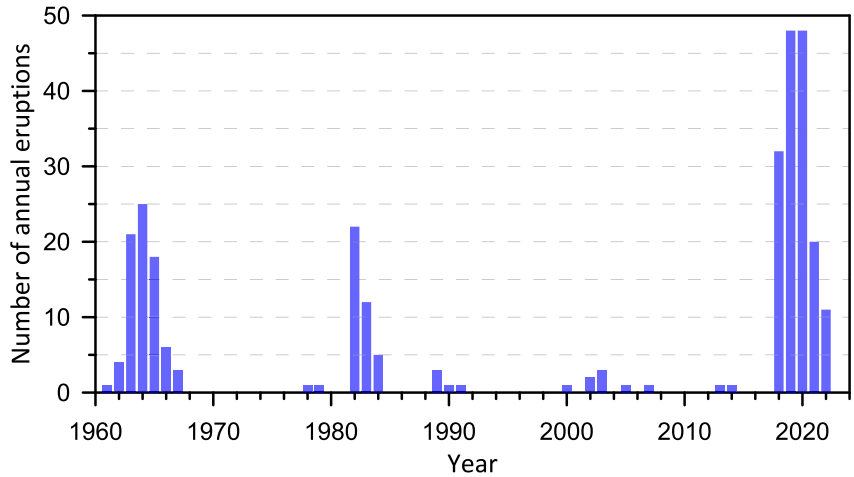

Figure 2. Annual count of major eruptions at Steamboat Geyser since 1961, which was preceded by a 50-year eruption dormancy. Data are from GeyserTimes (https://geysertimes.org/) and include 301 eruptions through 2022. This database reports 85 eruptions in the 1960s, likely representing an undercount and differing from the 104 eruptions reported by White et al. (1988).

Geyser active phases in multiple databases. Due to the bright color of the hydrothermal ground, some images were overexposed, which obscured the precise location of tree lines surrounding hydrothermally altered substrate. We located at least two aerial photos that bracket, or nearly bracket, each active phase (Figure 3). Low-resolution grayscale images from 1954 to 31 August 1965 and higher resolution images taken on 27 September 1978 and 4 September 1986 were obtained from Yellowstone National Park archival records. The 24 September 2015, 18 August 2019, and 19 July 2022 images were sourced from the National Agriculture Imagery Program (NAIP) at 0.5, 0.6, and 1.0 m resolution, respectively. Because the archival photographs lacked accompanying information to derive coordinates, we georeferenced the scanned images by assigning approximate point coordinates to thermal features, building corners, and trail and road intersections that remained stable through time.

The photographs in Figure 3a show possible minor changes to the tree line in the immediate vicinity of Steamboat Geyser by August 1965. At least 75% of the eruptions during the 1960s had occurred by this time. Though the low resolution and lack of color in these images make it difficult to identify stressed trees, ground-based photographs of the vent area indicate increased discoloration of trees to the east and northeast between 1962 and 1963 (Johnson & U.S. National Park Service, 1962–1963). Figure 3b indicates a similar story for the 1980s active phase, with possible tree death near the runoff channel to the south but no large variations in the tree line.

In contrast, widespread tree mortality has occurred during the recent active phase, and trees have been killed as far as 250 m away from the vents (Figure 3c), although as discussed in Section 8, tree mortality at distances greater than about 30 m from the geyser may have resulted from an increase in ground temperature rather than spray from the erupted water. The affected area covered 3.25×10^{-2} km^2 in August 2019, which marked 1.4 years and 64 eruptions into the active phase. Most of this mortality occurred north of Steamboat Geyser, which reflects the dominant southerly wind in the area. By July 2022, or 4.3 years and 156 eruptions into the active phase, the affected area expanded to the south and east and increased by 31% to 4.25×10^{-2} km^2. Note that the areas listed here include open thermal ground and clusters of trees that were already dead or dying in 2015 and therefore do not quantify the total tree kill due to Steamboat Geyser's eruptions.

4. Sample Collection

The collection area of silicified wood samples is a distinct 22 m × 6 m sinter platform located southeast to south of the Steamboat Geyser vent (Figure 1b). We sampled 20 wood remnants with various degrees of silica mineralization (Figure 4) in September 2021 and April 2022, within 5–14 m of the geyser vent. Sample weights ranged from 15 to 20 g. The full assemblage of mineralized wood at this site consists of at least 30 obvious small stem remnants ranging from 1 to 48 cm in length; there are additional less obvious remnants less than 2 cm in length. The majority of sampled remnants were partly entombed in sinter, and four sampled remnants (SGE107, SGE111, SGE115, SGE116) were loose on the sinter platform. We were unable to separate individual annual

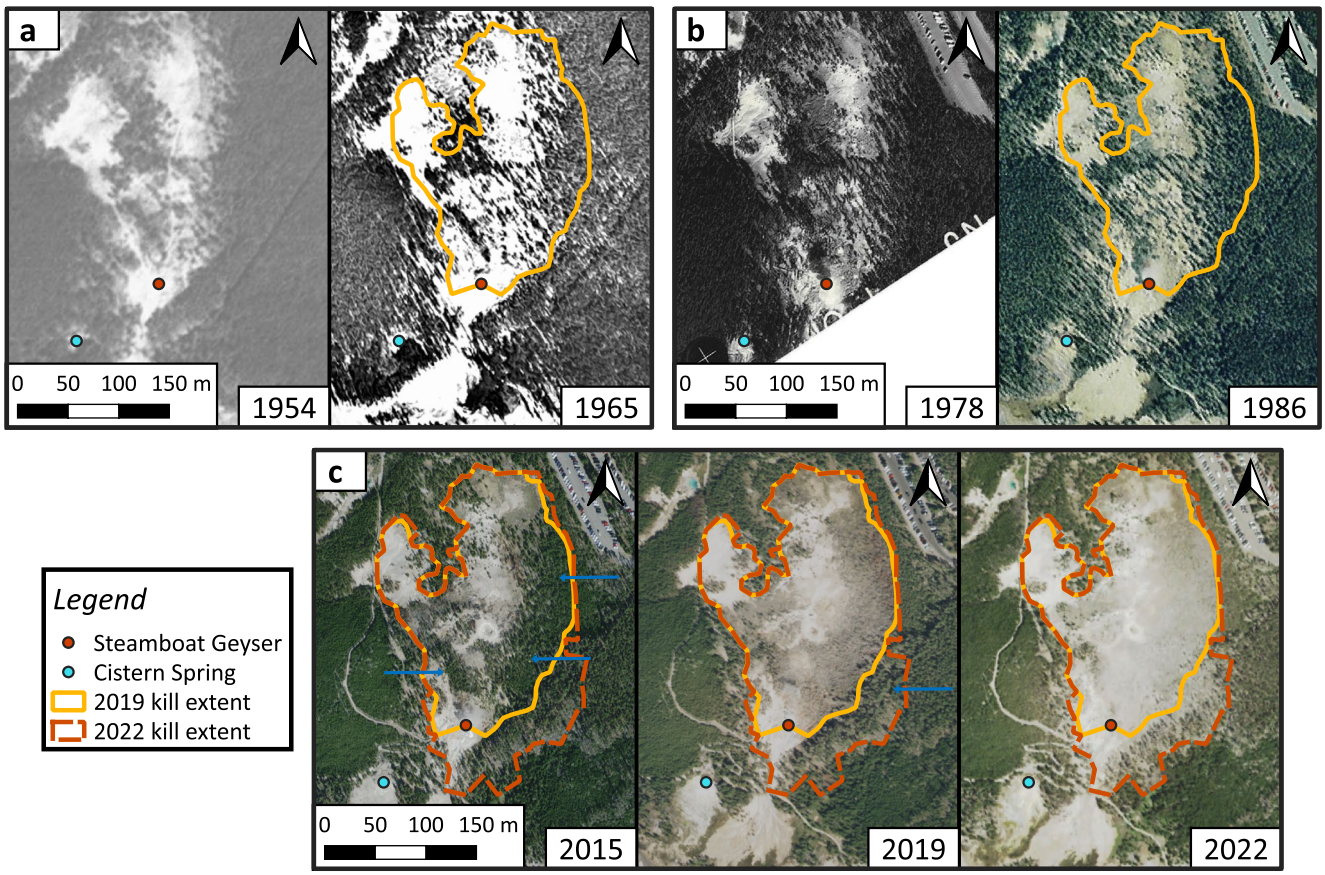

Figure 3. Aerial photographs showing areas with impacted trees around Steamboat Geyser. (a) Between1954 and 31 August 1965 (Aerial Photograph Collection (RG 01–26, Series I and RG 01–26, Box 22, Yellowstone National Park Archives, Yellowstone Heritage and Research Center, Gardiner, MT, United States)), (b) between 27 September 1978 and 4 September 1986 (Falcon Air Maps—https://pubs.nps.gov/Default.aspx?DocID=1788632), and (c) 24 September 2015, 18 August 2019, and 19 July 2022 (U.S. Department of Agriculture—https://gdg.sc.egov.usda.gov/GDGHome_DirectDownLoad.aspx). The photographs indicate minor changes to the tree line during the 1960s and 1980s active phases and major changes during the recent period of activity. White notations in the lower portion of the 1978 image in (b) were left unchanged from the original document. All panels in (c) show the approximate boundary of damaged trees in 2019 and 2022. The blue arrows point to areas where trees were impacted from the sequence of eruptions that began in March 2018.

rings from any of the samples. Three samples (SGE101, SGE105, SGE116) with low levels of silica mineralization were identified as lodgepole pine (*Pinus contorta* Dougl. var. *latifolia* Engelm.). The remaining highly friable mineralized samples lacked the cellular definition needed for species identification.

Increment core samples were collected from five of the oldest live lodgepole pine within 20–42 m of the Steamboat Geyser vent (trees with SG designation in Figure 1b). Core samples were processed using standard dendrochronological techniques and finely surfaced to clarify cell and ring structure (Stokes & Smiley, 1968; Swetnam et al., 1985). Chronological control was established using a lodgepole pine chronology (King, 2014) assembled from trees located approximately 1.2 km west of Steamboat Geyser (lodgepole pine tree-ring chronology Norris Upland Chronology (NUP)). Three cross-dating techniques were employed to establish exact calendar year dating in tree-ring samples: direct side-by-side microscopic comparison of tree-ring samples, skeleton plot matching (Stokes & Smiley, 1968; Swetnam et al., 1985), and correlation pattern techniques (Grissino-Mayer, 2001; Holmes et al., 1986). Five large, old trees with cambial dieback (CD designation in Figure 1b) were sampled. Two other large, old trees with unsampled cambial dieback designation in Figure 1b were not sampled. We have also documented 21 live trees that are less than 20 years old, are less than 0.7 m tall, and have well-defined dead canopy tops (trees with ST designation in Figure 1b).

5. Radiocarbon Dating Methods of Partially Mineralized Wood and Results

Radiocarbon dating of the mineralized wood and stable carbon isotope analyses ($\delta^{13}C$) were performed at the National Ocean Sciences Accelerator Mass Spectrometry facility at the Woods Hole Oceanographic Institution.

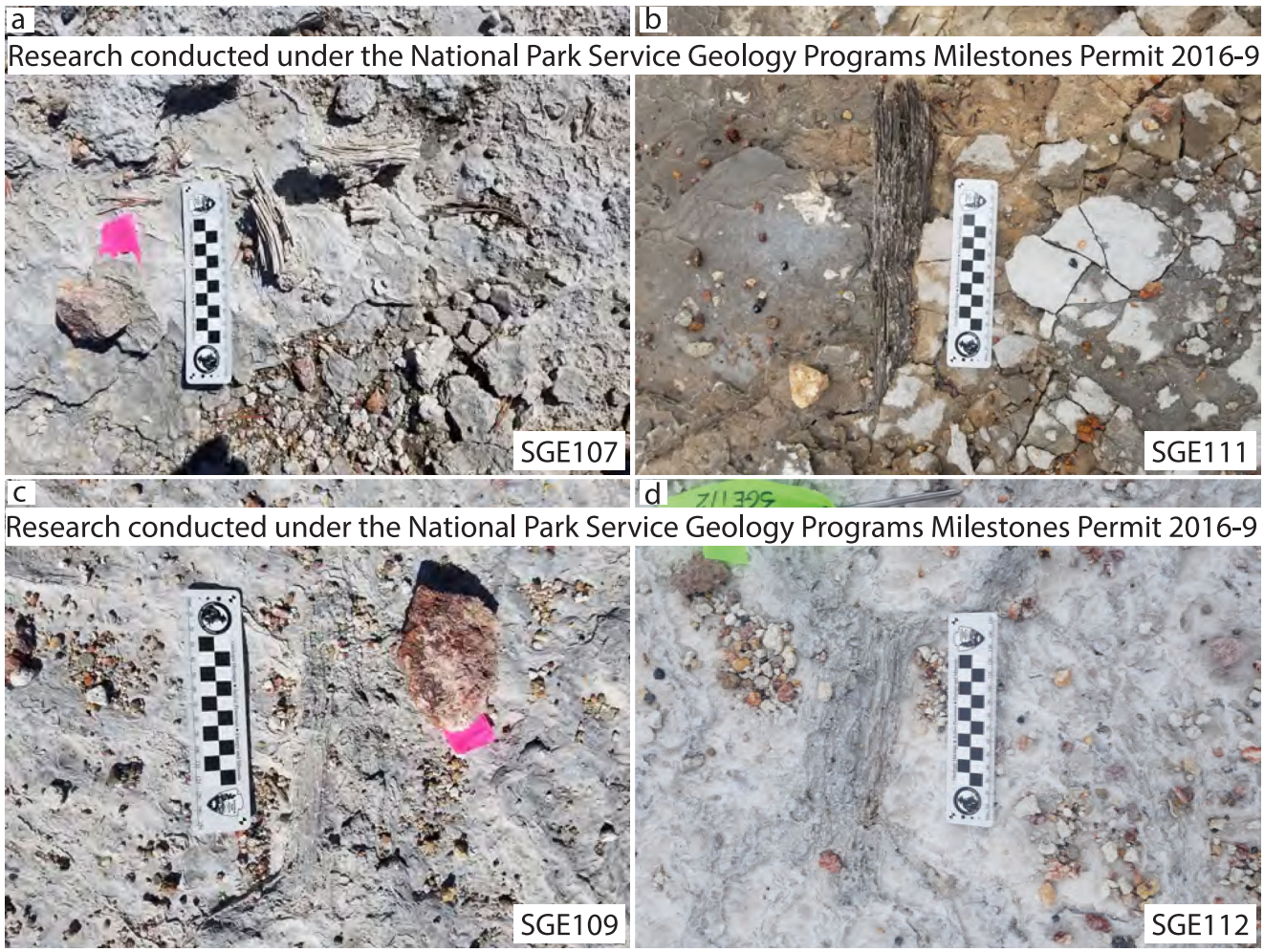

Figure 4. Photos of representative in situ partly mineralized wood samples (a) SGE107, (b) SGE111, (c) SGE109, and (d) SGE112. Each black and white square in the ruler is 1 cm.

A summary of the data is presented in Table 1 and in the data release (Hurwitz et al., 2023). The several plausible ^{14}C ages in Table 1 are relative to 1950 (BP; 0 yr BP = 1950 CE), and the uncertainties on the ages are given at the 95% (2σ) confidence level. The $\delta^{13}C$ values were normalized to the Vienna Pee Dee Belemnite (VPDB) standard and were not used for age corrections. The ^{14}C dates have been calibrated using the Bchron Package (Haslett & Parnell, 2008) within the program R (R version 4.0.5; R Development Core Team, 2022), which uses a continuous Markov monotone stochastic process to make inference on a partially observed monotone stochastic process. We used the "intcal20" calibration curve (Reimer et al., 2020) as input to the model. The probability density functions were generated by randomly calibrating the ^{14}C date and uncertainty range of each sample against the intcal20 curve 10,000 times.

None of the specimens had more than 20 annual rings, suggesting that the samples represent relatively short periods of growth in young trees, since lodgepole pines can live for more than a century in Yellowstone National Park. Samples SGE-117 and SGE-118 yielded modern ages and were excluded from further analysis. The rest of the samples (n = 18) yielded uncorrected ages of between 175 years (SGE-119) and 460 years (SGE-120). The $\delta^{13}C$ values of 17 samples ranged between (−21.65 and −27.40‰), which is mostly within the range expected for tree cellulose and lignin (−21 to −26‰; Loader et al., 2003), indicating negligible contamination by dissolved inorganic carbon, which in the Yellowstone hydrothermal system has values ranging between −4.7 and −0.7‰ (Bergfeld et al., 2019). Sample SGE-106 did not have sufficient material for $\delta^{13}C$ analysis. Contamination by old carbon sources in sinter organic carbon can be recognized by anomalously heavy $\delta^{13}C$ (e.g., Churchill et al., 2020; Munoz-Saez et al., 2020).

Geochemistry, Geophysics, Geosystems

10.1029/2023GC010988

Table 1
Summary of the Radiocarbon Ages and Probabilities

Sample[a]	Age years[b]	Error ±[c]	$\delta^{13}C$[d] ‰	P1[e] Min	P1 Max	Median year	%	P2 Min	P2 Max	Median year	%	P3 Min	P3 Max	Median year	%	P4 Min	P4 Max	Median year	%	P5 Min	P5 Max	Median year	%
SGE-101	275	15	−25.07	291	318	1646	15.7	383	383	1567	1.0	392	424	1542	**78.4**[f]								
SGE-102	205	20	−22.89	0	13	1944	3.4	16	21	1932	1.7	148	190	1781	23.7	194	216	1745	20.9	267	299	1667	**45.5**
SGE-103	295	25	−26.10	293	332	1638	11.5	354	445	1551	**83.6**	–	–	–	–	–	–	–	–	–	–	–	–
SGE-104	320	20	−24.21	310	335	1628	8.1	337	339	1612	1.3	349	454	1549	**85.7**	–	–	–	–	–	–	–	–
SGE-105	225	15	−25.06	0	7	1947	2.0	153	171	1788	13.7	179	182	1770	5.4	279	305	1658	**73.9**	–	–	–	–
SGE-106	265	25	–	0	–	–	0.1	154	168	1789	2.3	283	327	1645	16.3	374	428	1549	**76.3**	–	–	–	–
SGE-107	315	20	−26.25	308	334	1629	7.9	350	451	1550	**86.2**	453	453	1497	1.1	–	–	–	–	–	–	–	–
SGE-108	370	20	−25.32	321	376	1602	24.3	388	388	1562	0.7	427	494	1490	**70.1**	–	–	–	–	–	–	–	–
SGE-109	495	20	−25.45	507	539	1427	**90.9**	–	–	–	–	–	–	–	–	–	–	–	–	–	–	–	–
SGE-110	430	20	−24.20	474	515	1456	**90.2**	–	–	–	–	–	–	–	–	–	–	–	–	–	–	–	–
SGE111	275	15	−24.36	291	318	1646	15.7	383	383	1567	1.0	392	424	1542	**78.4**	–	–	–	–	–	–	–	–
SGE112	435	20	−25.05	476	516	1454	**90.2**	–	–	–	–	–	–	–	–	–	–	–	–	–	–	–	–
SGE113	235	15	−21.65	0	2	1949	1.4	154	168	1789	17.7	283	306	1656	**75.9**	–	–	–	–	–	–	–	–
SGE114	275	20	−26.13	158	162	1790	0.9	288	321	1646	11.4	324	325	1626	1.2	376	427	1549	**81.6**	–	–	–	–
SGE115	235	15	−24.23	0	2	1949	1.4	154	168	1789	17.7	283	306	1656	75.9	–	–	–	–	–	–	–	–
SGE116	235	20	−23.04	0	8	1946	1.4	152	171	1789	7.1	178	183	1770	4.7	203	206	1746	4.2	279	311	1655	**77.7**
SGE117	>Modern	–	−27.40	–	–	–	–	–	–	–	–	–	–	–	–	–	–	–	–	–	–	–	–
SGE118	>Modern	–	−26.40	–	–	–	–	–	–	–	–	–	–	–	–	–	–	–	–	–	–	–	–
SGE119	175	15	−24.86	0	26	1937	12.1	142	154	1802	9.2	167	221	1756	**49.9**	262	284	1677	23.9	–	–	–	–
SGE120	460	15	−25.61	198	522	1590	**88.9**	–	–	–	–	–	–	–	–	–	–	–	–	–	–	–	–

[a]More analytical data are available at Hurwitz et al. (2023). [b]BP; 0 yr BP = 1950 A.D. [c]Uncertainties are given at the 95% (2sigma) confidence level. [d]Normalized to $\delta^{13}C$ VPDB. The $\delta^{13}C$ results were not used for correcting ^{14}C data. [e]The Bayesian software package Bchron (Haslett & Parnell, 2008) and the intcal20 calibration curve (Reimer et al., 2020) were used for calculating the age probability density functions. [f]Bold fonts indicate the mode with the highest probability.

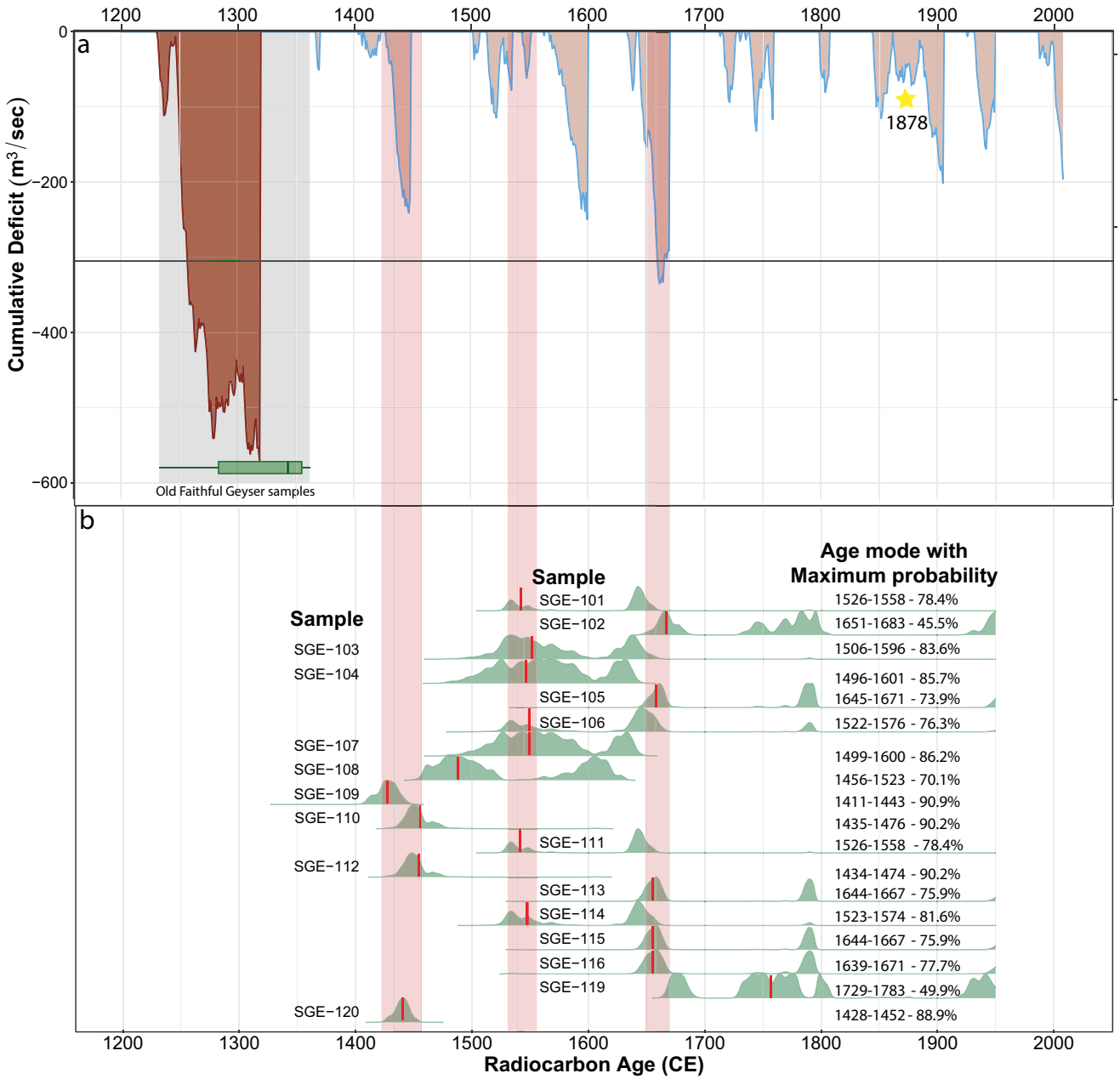

Figure 5. (a) The 1,200-year reconstruction of the cumulative streamflow deficits associated with the time period of each identified drought event (brown area). The gray rectangle shows the time period of the century megadrought in the 13th and 14th centuries and the eruption hiatus of Old Faithful Geyser (Hurwitz et al., 2020) represented by a boxplot showing the median-calibrated date and upper and lower quartiles of all ^{14}C dates from across the mineralized wood samples (in green). The yellow star denotes the previous estimate on the initiation of Steamboat Geyser in 1878. (b) Results from ^{14}C dating of silicified wood samples from around Steamboat Geyser. Details on the ^{14}C calibrations, the calculated probability density functions, and uncertainty calculations are described in detail in Section 5. The vertical red lines show the median of the most probable age mode, and the three pink rectangles delimit most of the medians (except for samples SGE-108 and SGE-119). Data are provided in Table 1 and in Hurwitz et al. (2023).

The calibrated ^{14}C dates resulted in one to five possible modes for each of the samples, each having a different age range and a different probability. Multiple modes are a consequence of more than one possible match between ^{14}C dates with the ^{14}C calibration curve ("wiggle matching"). The pattern generated by the highest probability mode for each sample suggest that specimens mainly cluster in three periods: the late 15th Century, mid-17th Century, and late 18th Century (Table 1, Figure 5).

Table 2
Information on Cores Collected From Trees Surrounding Steamboat Geyser

Tree ID	Distance from vent (m)[a]	Establishment year	Notes
SG1	20	1874	1965 light latewood ring
SG2	21	Unknown	Possibly 2 absent rings
			Likely >120-yr-old
SG3	25	1871	2 absent rings near 2019
			1965–1972 suppressed growth
SG4	42	1872	2020 extremely small growth ring

[a]Tree locations are shown in Figure 1b.

6. Pathology of Live Trees Surrounding Steamboat Geyser

Both young and old live trees growing within 30 m southwest to south of the geyser vent display cambial dieback that does not appear on other trees in the vicinity of Steamboat Geyser. The estimated establishment dates of three trees (SG1, SG3, SG4; Figure 1b) cluster in the early 1870s (Table 2). We compared the standardized tree-ring indices of trees SG3 and SG4 to the index of a lodgepole chronology (NUP) that is located 1.2 km to the west of Steamboat Geyser and is not impacted by its eruptions (Figure 6). The NUP chronology ends in 2009 and therefore does not cover the period of geyser activity that started in March 2018. The 1965 light latewood ring in tree SG1 and the greatly reduced growth in tree SG3 coincide with the 1961–1969 major eruption episode. Absent tree-rings are discovered through the process of statistical and visual cross dating against trees unaffected by geyser activity. The two absent rings near 2019 in tree SG3 and the extremely small 2020 growth ring in tree SG4 coincide with the 2018–2021 major eruption episode. These observations suggest an ongoing negative effect of recent geyser activity on lodgepole pine growth, possibly extending back to at least the early 1870s.

The closest forest edge to Steamboat Geyser is located 14 m southeast to 24 m south of the geyser vent. Along this edge, and extending approximately 12 m into the forest, both old and young lodgepole pine exhibit signs of cambial dieback that are not seen farther to the southeast or south. At least six of the oldest and largest (30–50 cm diameter at breast height) live trees (SG1, SG2, SG3, CD4, CD5, CD6) have large, dead branches and/or vertical strips of dead cambium. Tree tops with large, dead branches and trees with strips of exposed wood (cambial dieback) can be associated with old trees with growth often spanning multiple centuries or more (Fritts, 1976). At least 18 live trees (ST1-ST18) less than 20-yr-old and less than 0.7 m tall have well-defined dead canopy tops.

The second closest forest edge to Steamboat Geyser is 27 m southwest of the geyser vent. In this vicinity, three live trees (ST19-ST21) less than 0.7 m tall were found to have dead canopy tops; the oldest apparent tree (SG4) is 40 m southwest of the geyser vent. The cambial dieback seen on both young and old lodgepole pine adjacent to Steamboat Geyser does not appear on other trees in this region. Overall, the pattern of tree damage is most consistent with effects dominated by spray, mostly downwind of Steamboat Geyser. Subsurface and surface flows of geothermal fluids move southward from the geyser, away from the area with greatest tree damage.

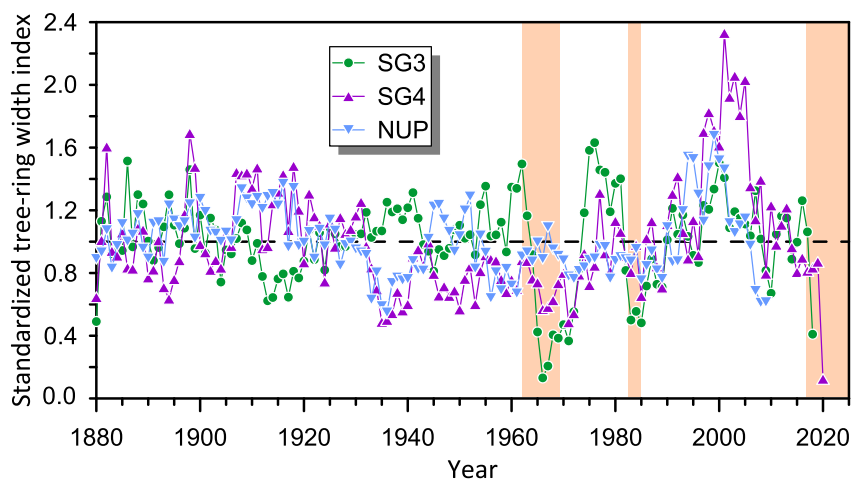

Figure 6. Standardized tree-ring-width indices for the local (Norris Geyser Basin) lodgepole pine chronology (Norris Upland Chronology [NUP]) growing away from Steamboat Geyser, and for two trees growing adjacent to Steamboat Geyser (SG3, SG4; Figure 1b). The dashed horizontal line represents the mean-standardized index value for the period. The orange rectangles delimit the three episodes in which most major Steamboat Geyser eruptions occurred.

7. Reconstructed Multidecadal Drought Events for the Yellowstone Region

To assess potential hydroclimatic drivers associated with hiatuses of Steamboat Geyser eruptions, we assessed the relationship between the calibrated ^{14}C dates and tree-ring-based reconstruction of annual water-year streamflow and drought for the Yellowstone River (Figure 5a) (Martin et al., 2019b). Here, we provide a summary of the methods used to identify long-duration droughts and calculate their cumulative deficits, with further details provided in Hurwitz et al. (2020). The primary record used is the 1,200-year reconstruction of mean annual water-year (prior October–September) streamflow for the Yellowstone River at Corwin Springs, Montana (YCR in Figure 1a). This record reflects the regional total annual moisture balance, capturing the dominant influence (~50%–80%) of cool-season (October–April) precipitation on regional surface and groundwater hydrology (Martin et al., 2019a) for the Yellowstone region. As a final check on inferred local moisture conditions, we also compare against the predominantly spring (May–June) precipitation sensitive Rocky Mountain Juniper (*Juniperus scopulorum*, Sarg.) standardized ring-width chronology from King (2016), known as Chinese Garden Expanded, using methods designed to preserve low-frequency hydroclimatic variability described in Martin et al. (2019a). For comparison of the records, and to identify the relative magnitude and duration of associated multi-decadal moisture anomalies, all records were smoothed using a 50-year cubic smoothing spline (Figure 5a) before the cumulative deficits of identified drought events were calculated (Figure 5b). Using smoothing splines with shorter duration (10 or 20 years) changed the estimated length and magnitude of individual droughts but did not significantly alter the identification of severe and long-duration drought events over past centuries.

Multidecadal drought periods for the Yellowstone River at Corwin Springs reconstruction were identified as periods of negative flow anomalies in the 50-yr cubic smoothing spline of streamflow. With drought length defined by the negative flow anomaly of the spline, cumulative streamflow deficits were calculated for each drought period by summation of the unsmoothed annual flow values for each year of the drought (Martin et al., 2020). The "megadrought" event of record responsible for the eruption hiatus at Old Faithful Geyser occurred in the 13th century and was greater than 50 years in duration, with the most severe drought years centered on the year 1250 CE (Figure 5a). Several shorter durations but still large-magnitude severe droughts are also apparent in the reconstruction and occur between the 15th and 17th centuries (Figure 5a). Of these events, the drought of the late 16th century was one of the most notable in terms of the severity of negative effects on people and ecosystems along with its broad spatial extent across the western United States. These droughts led to more fires, desiccation of small lakes, reduced streamflow, and an upslope shift in upper tree line (Hostetler et al., 2021; Williams et al., 2020).

8. Discussion

Lodgepole pine trees dominate ~80% of the total forested area in Yellowstone National Park, including the trees surrounding Steamboat Geyser, and the preponderance of its saplings over competing species indicates its resilience (Despain, 1983). Lodgepole pine exposed to silica-rich alkaline thermal waters can be preserved for many centuries (e.g., Hellawell et al., 2015; Hurwitz et al., 2020; Liesegang & Gee, 2020), most likely because silica precipitation prevents the disintegration of cellulose by fungi, bacteria, and insects. In Yellowstone National Park's nonthermal areas where trees are not exposed to silica-rich waters, lodgepole pine deadwood is mostly not preserved for more than 300 years (Despain, 1983). Alkaline chloride-rich waters discharged by geyser eruptions can become supersaturated with respect to silica, resulting in the deposition of colloidal amorphous opal on trees. Silica mineralization initiates when amorphous opal is deposited on tree stems, and this coating enables the transport of silica-rich fluids into wood tissues by capillary forces (Liesegang & Gee, 2020). Silica is then preferentially deposited in small pore spaces including pit chambers, latewood tracheid lumina, and parenchyma rays (Mustoe, 2017). A study of upright, dead saplings near Cistern Spring (Figure 1b) indicated that mineralization lasting days to weeks would be sufficient to cause mortality (Liesegang & Gee, 2020). Based on these observations, and on the observations from Old Faithful Geyser (Hurwitz et al., 2020), we infer that discontinuous growth of trees proximal to geysers is indicative of changes in eruptive patterns, with trees establishing and growing during periods of geyser inactivity.

Photographic evidence indicates that trees up to 250 m north of the Steamboat Geyser vent were impacted before 1954 (Figure 3a). The size of the impacted area (outline in Figure 3) did not change considerably between 1954 and 2015, suggesting that water spray and silica precipitation from Steamboat Geyser eruptions in the 1960s and 1980s did not have much impact on the growth of trees that surround the geyser. However, the eruption sequence

that started in March 2018 clearly had an adverse impact on trees up to at least 30 m from the geyser vent, as indicated by the area between the orange and red outlines and by the blue arrows in Figure 3c. A possible explanation for the different response of trees to the active phases during the 1960s and 1980s and the response to the post-2018 active phase lies in the amount and frequency of major eruptions during the different active phases (Figure 2). The average annual number of eruptions in 1963–1965 (21 annual eruptions) and in 1982 and 1983 (11 annual eruptions) is significantly less than the annual average number of eruptions between in 2018–2020 (43 eruptions). Thus, we hypothesize that lodgepole pine mortality depends on how often the trees are in the path of falling spray from the erupting geyser. Another potential impact on active eruption phases and atypical tree growth is local and short-lived increases in shallow ground temperatures. Although an increase in ground temperature may better explain the impacts on tree growth at distances greater than about 30 m from Steamboat Geyser (rather than spray from the erupted water), there are no data to test this hypothesis.

Despite the significant challenges of using ^{14}C for dating charcoal and pollen to provide constraints on the timing of processes in Yellowstone's hydrothermal system (Churchill et al., 2020; Schiller et al., 2021), analysis of tree-rings and ^{14}C dating of tree remnants in active volcanic settings have provided reliable records on past hydrothermal activity (Cook et al., 2001; Holdaway et al., 2018; Lewicki et al., 2014), including information on activity changes in Yellowstone National Park's thermal areas (Evans et al., 2010; Hurwitz et al., 2020). The new ^{14}C data presented in our study of tree remnants collected around Steamboat Geyser are complex but nevertheless provide information on when Steamboat Geyser was active and on possible geyser response to periods of extended drought.

There are several indicators that the silicified tree remnant samples were in situ. Photographs of the sampling site since the 1950s, particularly during and following major eruption episodes, do not show evidence of recently deposited wood (Figure 3). This observation suggests that it is unlikely that the now mineralized wood originated upslope and moved into place with surface water runoff. Also, if the tree remnants were transported from a great distance (by wind or floods, e.g.,) to near the geyser vent on the sinter platform, a more randomized distribution of ^{14}C ages would be expected. However, the calibrated ^{14}C dates of tree remnants from around Steamboat Geyser are discontinuous and mainly cluster around three episodes. Based on tree-ring patterns, none of the silicified tree remnants suggest that trees grew for extended periods (many tens to hundreds of years). These observations suggest a causal relation between geyser activity and tree growth. The ^{14}C age clusters mostly overlap with three periods of drought in the Yellowstone region (Figure 5). The most probable calibrated dates of 16 samples are between 1410 and 1460 CE, 1530 and 1590 CE, and 1635 and 1670 CE. These dates of tree growth around Steamboat Geyser coincide with lake sediment proxy records of droughts and large fires in the region (Millspaugh & Whitlock, 1995). The median dates of some (but not all) of the highest probable calibrated modes from the samples we analyzed are within the drought period in the late 16th century, which was severe across much of the western United States (Martin et al., 2020; Williams et al., 2020).

Though the duration and severity of these drought periods rank as some of the most significant events within the record, they pale in comparison to the 13th century drought that led to the quiescence of Old Faithful Geyser toward the end of the Medieval Climate Anomaly (Figure 5) (Hurwitz et al., 2020). There are several possible explanations for why remnants of trees from the end of the Medieval Climate Anomaly were not found around Steamboat Geyser: either the geyser had not formed yet, tree remnants were either covered by younger sinter deposits or were eroded, or that the geyser was erupting during that time. This last possibility is inconsistent with our hypothesis that geysers tend to become quiescent during severe and extended droughts.

The most probable calibrated dates for two samples, SGE-108 and SGE-119, are not within these three drought periods (Figure 5b). The probability for the most likely age mode for sample SGE-119 (187–221 years) is relatively low (49.9%), but the next most probable mode (262–284 years with a probability of 23.9%) would suggest a median age of 1677 CE, which is within analytical uncertainty similar to the youngest cluster (1635–1670 CE). Two samples (SGE-117 and SGE-118) yielded modern ages (Hurwitz et al., 2023), and we suspect that these are from trees that possibly died in 1878 or later. Overall, our findings in relation to major regional droughts are consistent with other regional paleoclimate records (Cook et al., 2004; Heeter et al., 2021; Hostetler et al., 2021; Shuman & Serravezza, 2017; Turner et al., 2022; Whitlock et al., 2012; Williams et al., 2020).

Despite the strong evidence for trees growing around Steamboat Geyser when it was not erupting during extended and severe droughts, instrumental snow records in NGB and streamflow data do not correlate with the onset or termination of the three modern eruptive episodes of Steamboat Geyser (Figure 7). River discharge data from the USGS gages on the YCR (USGS 06191500; U.S. Geological Survey, 2022) and the Madison River near West Yellowstone, Montana (USGS 06037500; U.S. Geological Survey, 2022) have been shown to correlate with

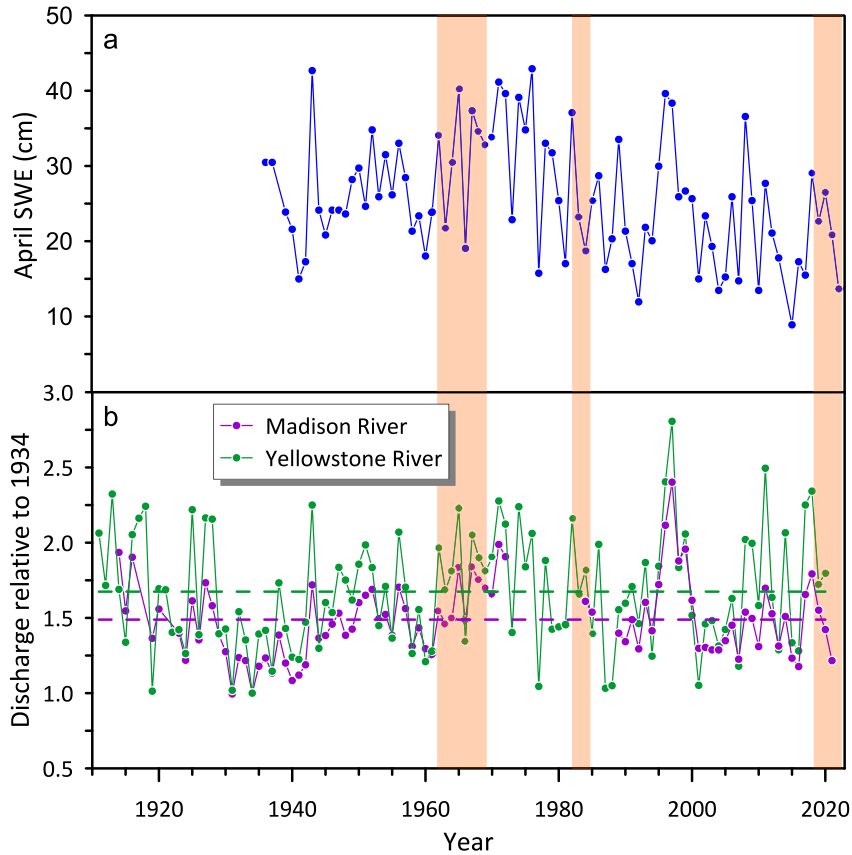

Figure 7. (a) Snow Water Equivalent in the month of April measured at station 10E19 in Norris Geyser Basin by the US Department of Agriculture, Natural Resources Conservation Service (https://wcc.sc.egov.usda.gov/nwcc/rgrpt?report=snowmonth_hist&state=WY), (b) annual average water discharge measured at USGS gages on the Yellowstone River at Corwin Springs, Montana (green curve and symbols; YCR in Figure 1a; USGS 06191500; U.S. Geological Survey, 2022) and the Madison River near West Yellowstone, Montana (purple curve and symbols; YMAD in Figure 1a; USGS 06037500; U.S. Geological Survey, 2022). The green and purple dashed horizontal lines show the annual means for the period for the Yellowstone and Madison Rivers, respectively. The orange rectangles delimit the three episodes in which most major Steamboat Geyser eruptions occurred.

precipitation in the Yellowstone Plateau on monthly and annual timescales (Hurwitz et al., 2007, 2008). However, years of high snow precipitation or river discharge do not correlate with the onset or duration of the three major eruptive phases (Figure 7). The absence of a clear correlation between periods of eruptive activity in the 20th and 21st centuries and climate suggests that longer and more severe droughts, or other processes, are needed to cause Steamboat Geyser to stop erupting for extended periods so that trees could establish and grow near the vent. A range of processes were examined by Reed et al. (2021) in search of a possible trigger for the March 2018 reactivation of Steamboat Geyser. There were no regional (Hurwitz et al., 2014) or remote (Husen et al., 2004) earthquakes that were a combination of large enough and close enough that they could have initiated the onset of eruptions. Interaction with adjacent geysers (Fagan et al., 2022) is also ruled out because there are no large active geysers in the vicinity of Steamboat that could impact its activity. It was postulated that transitions from dormant to eruptive periods at Steamboat Geyser may reflect gradual changes in silica precipitation in the reservoir or conduit that affect permeability, water flow, and heat transport (Reed et al., 2021). Direct observations of such a process are lacking.

9. Conclusions

We examined the response of Steamboat Geyser in Yellowstone National Park's NGB to decadal and multidecadal drought events. Based on the diverse and complementary data sets presented, we conclude the following:

1. Aerial and ground photographs indicate that prior active eruptive phases of Steamboat Geyser have adversely affected nearby trees. Some periods of activity can affect trees at significant distances from the vents, suggesting

that significant eruption episodes may be accompanied by temporary shallow hydrothermal changes in the local area, as well as from spray dispersal primarily in the dominant wind direction.

2. The most probable calibrated radiocarbon dates of 16 samples of silicified trees collected from around the Steamboat Geyser vent are clustered within three periods: between and 1410 and 1460 CE, 1530 and 1590 CE, and 1635 and 1670 CE. This discontinuous growth of trees is probably indicative of changes in geyser eruptive patterns, with trees growing during periods of geyser inactivity.
3. The clustered radiocarbon age distribution is supported by the observation that none of the silicified specimens had more than 20 annual rings, which likely suggests relatively short periods of tree growth and with the observations of atypical or missing rings in live trees during periods of recent geyser activity.
4. The periods when trees grew on the geyser mound are temporally correlated with periods of prolonged drought in the Yellowstone region during the 15th to 17th centuries. However, none of these droughts was as severe as the prolonged drought during the Medieval Climate Anomaly in the 13th and 14th centuries that caused Old Faithful Geyser in Yellowstone National Park's UGB to cease erupting for more than a century (Hurwitz et al., 2020).
5. The new radiocarbon dates of silicified trees most likely invalidate the prior assertion that the geyser was formed in 1878.

Overall, the link between drought, geyser inactivity, and tree growth at both Old Faithful (Hurwitz et al., 2020) and Steamboat Geysers suggests that Yellowstone's hydrothermal system and activity of its geysers systematically respond to changes in regional precipitation patterns at the decadal to millennial timescales.

Conflict of Interest

The authors declare no conflicts of interest relevant to this study.

Data Availability Statement

Steamboat Geyser eruption data can be obtained via https://geysertimes.org/retrieve.php. Tree-ring data can be obtained via King (2023). All other data presented in this study are publicly available in USGS data releases. The Yellowstone River at Corwin Springs streamflow reconstruction is available in Martin et al. (2019b) and the radiocarbon data are available in Hurwitz et al. (2023). Original scanned aerial photographs (Figure 3) from 1954 to 1965 can be viewed by appointment at the Yellowstone Heritage and Research Center in Gardiner, Montana, USA. Photographs from 1978 to 1986 can be viewed in the U.S. National Park Service Electronic Technical Information Center at https://pubs.nps.gov/Default.aspx?DocID=1788632. Aerial photos from the National Agriculture Imagery Program (NAIP) can be downloaded via USGS EarthExplorer (https://earthexplorer.usgs.gov/) or in compressed county mosaic format from the U.S. Department of Agriculture (USDA) Geospatial Data Gateway (https://datagateway.nrcs.usda.gov/GDGHome_DirectDownLoad.aspx). Streamflow gaging data are available from U.S. Geological Survey (2022).

Acknowledgments

This study was conducted under the National Park Service Geology Programs Milestones Permit 2016–2019. We thank Annie Carlson from the Yellowstone Center for Resources for help with logistics. Janet Jones is thanked for providing the aerial photo used in Figure 1. Sady King is thanked for field work assistance. Patrick Muffler, Silvina Slagter, and an anonymous reviewer are thanked for their constructive comments. Any use of trade, firm, or product names is for descriptive purposes only and does not imply endorsement by the U.S. Government. MM and MHR are supported by the National Science Foundation 2116573 and CIFAR Earth 4D.

References

Barrick, K. A. (2007). Geyser decline and extinction in New Zealand—Energy development impacts and implications for environmental management. *Environmental Management*, *39*(6), 783–805. https://doi.org/10.1007/s00267-005-0195-1

Bergfeld, D., Lowenstern, J. B., Hunt, A. G., Hurwitz, S., McCleskey, B. R., & Peek, S. E. (2019). *Chemical and isotopic data on gases and waters for thermal and non-thermal features across Yellowstone National Park (version 2.0, March 2019)*. U.S. Geological Survey Data Release. https://doi.org/10.5066/F7H13105

Blanchette, R. A. (1995). Degradation of the lignocellulose complex in wood. *Canadian Journal of Botany*, *73*(S1), 999–1010. https://doi.org/10.1139/b95-350

Christiansen, R. L., (2001). The quaternary and Pliocene Yellowstone Plateau volcanic field of Wyoming, Idaho, and Montana. US Geological Survey Professional Paper 729-G. (p. 120). https://doi.org/10.3133/pp729G

Churchill, D. M., Manga, M., Hurwitz, S., Peek, S., Licciardi, J. M., & Paces, J. B. (2020). Dating silica sinter (geyserite): A cautionary tale. *Journal of Volcanology and Geothermal Research*, *402*, 106991. https://doi.org/10.1016/j.jvolgeores.2020.106991

Cook, A. C., Hainsworth, L. J., Sorey, M. L., Evans, W. C., & Southon, J. R. (2001). Radiocarbon studies of plant leaves and tree rings from Mammoth Mountain, CA: A long-term record of magmatic CO_2 release. *Chemical Geology*, *177*(1–2), 117–131. https://doi.org/10.1016/S0009-2541(00)00386-7

Cook, E. R., Woodhouse, C. A., Eakin, C. M., Meko, D. M., & Stahle, D. W. (2004). Long-term aridity changes in the Western United States. *Science*, *306*(5698), 1015–1018. https://doi.org/10.1126/science.1102586

Despain, D. G. (1983). Nonpyrogenous climax lodgepole pine communities in Yellowstone National Park. *Ecology*, *64*(2), 231–234. https://doi.org/10.2307/1937070

Evans, W. C., Bergfeld, D., McGeehin, J. P., King, J. C., & Heasler, H. (2010). Tree-ring ^{14}C links seismic swarm to CO_2 spike at Yellowstone, USA. *Geology*, *38*(12), 1075–1078. https://doi.org/10.1130/G31345.1

Fagan, W. F., Swain, A., Banerjee, A., Ranade, H., Thompson, P., Staniczenko, P. P., et al. (2022). Quantifying interdependencies in Geyser Eruptions at the Upper Geyser Basin, Yellowstone National Park. *Journal of Geophysical Research: Solid Earth*, *127*(8), e2021JB023749. https://doi.org/10.1029/2021JB023749

Fournier, R. O., Weltman, U., Counce, D., White, L. D., & Janik, C. J. (2002). Results of weekly chemical and isotopic monitoring of selected springs in Norris Geyser Basin, Yellowstone National Park during June–September 1995. US Geological Survey Open-File Report, 344. Retrieved from https://pubs.usgs.gov/of/2002/0344

Fritts, H. (1976). *Tree rings and climate*. Academic Press. https://doi.org/10.1038/scientificamerican0572-92

Gaspard, F., Opfergelt, S., Hirst, C., Hurwitz, S., McCleskey, R. B., Zahajská, P., et al. (2021). Quantifying non-thermal silicate weathering using Ge/Si and Si isotopes in rivers draining the Yellowstone Plateau volcanic field, USA. *Geochemistry, Geophysics, Geosystems*, *22*(11), e2021GC009904. https://doi.org/10.1029/2021GC009904

Gastellum, L. A., (1963). Description of eruption of Steamboat Geyser as observed by Luis A. Gastellum, Associate Superintendent December 25, 1962. Geology Program Records (Box 82).

Grissino-Mayer, H. D. (2001). FHX2-software for analyzing temporal and spatial patterns in fire regimes from tree rings. *Tree-Ring Research*, *57*, 115–124.

Haslett, J., & Parnell, A. (2008). A simple monotone process with application to radiocarbon-dated depth chronologies. *Journal of the Royal Statistical Society*, *57*(4), 399–418. https://doi.org/10.1111/j.1467-9876.2008.00623.x

Hayden, F. V. (1883). Twelfth annual report of the United States geological and geographical survey of the territories: A report of progress of the exploration in Wyoming and Idaho for the year 1878, part II: Yellowstone National Park. *United States Geological Survey*. https://doi.org/10.3133/70038941

Heeter, K. J., Rochner, M. L., & Harley, G. L. (2021). Summer air temperature for the Greater Yellowstone Ecoregion (770–2019 CE) over 1,250 years. *Geophysical Research Letters*, *48*(7), e2020GL092269. https://doi.org/10.1029/2020GL092269

Hellawell, J., Ballhaus, C., Gee, C. T., Mustoe, G. E., Nagel, T. J., Wirth, R., et al. (2015). Incipient silicification of recent conifer wood at a Yellowstone hot spring. *Geochimica et Cosmochimica Acta*, *149*, 79–87. https://doi.org/10.1016/j.gca.2014.10.018

Holdaway, R. N., Duffy, B., & Kennedy, B. (2018). Evidence for magmatic carbon bias in ^{14}C dating of the Taupo and other major eruptions. *Nature Communications*, *9*, 1–9. https://doi.org/10.1038/s41467-018-06357-0

Holmes, R. L., Adams, R. K., & Fritts, H. C. (1986). *Tree-ring chronologies of western North America: California, eastern Oregon and northern Great Basin*. Laboratory of Tree-Ring Research, University of Arizona.

Hostetler, S., Whitlock, C., Shuman, B., Liefert, D., Drimal, C. W., & Bischke, S. (2021). *Greater Yellowstone climate assessment: Past, present, and future climate change in greater Yellowstone watersheds* (p. 260). Montana State University, Institute on Ecosystems. Retrieved from https://scholarworks.montana.edu/xmlui/handle/1/16361

Hurwitz, S., Evans, W. C., & Lowenstern, J. B. (2010). River solute fluxes reflecting active hydrothermal chemical weathering of the Yellowstone Plateau Volcanic Field, USA. *Chemical Geology*, *276*(3–4), 331–343. https://doi.org/10.1016/j.chemgeo.2010.07.001

Hurwitz, S., King, J. C., Pederson, G. T., Martin, J. T., Damby, D. E., Manga, M., et al. (2020). Yellowstone's Old Faithful Geyser shut down by a severe thirteenth century drought. *Geophysical Research Letters*, *47*(20), e2020GL089871. https://doi.org/10.1029/2020GL089871

Hurwitz, S., King, J. C., Pederson, G. T., Reed, M. H., Harrison, L. N., Hungerford, J. D. G., et al. (2023). Radiocarbon dating of silicified wood from around Steamboat Geyser in Norris Geyser Basin, Yellowstone National Park, 2021-2022 [Dataset]. U.S. Geological Survey. https://doi.org/10.5066/P9NG2TF4

Hurwitz, S., Kumar, A., Taylor, R., & Heasler, H. (2008). Climate-induced variations of geyser periodicity in Yellowstone National Park, USA. *Geology*, *36*(6), 451–454. https://doi.org/10.1130/G24723A.1

Hurwitz, S., & Lowenstern, J. B. (2014). Dynamics of the Yellowstone hydrothermal system. *Reviews of Geophysics*, *52*(3), 375–411. https://doi.org/10.1002/2014RG000452

Hurwitz, S., Lowenstern, J. B., & Heasler, H. (2007). Spatial and temporal geochemical trends in the hydrothermal system of Yellowstone National Park: Inferences from river solute fluxes. *Journal of Volcanology and Geothermal Research*, *162*(3–4), 149–171. https://doi.org/10.1016/j.jvolgeores.2007.01.003

Hurwitz, S., & Manga, M. (2017). The fascinating and complex dynamics of geyser eruptions. *Annual Review of Earth and Planetary Sciences*, *45*(1), 31–59. https://doi.org/10.1146/annurev-earth-063016-015605

Hurwitz, S., Sohn, R. A., Luttrell, K., & Manga, M. (2014). Triggering and modulation of geyser eruptions in Yellowstone National Park by earthquakes, Earth tides, and weather. *Journal of Geophysical Research: Solid Earth*, *119*(3), 1718–1737. https://doi.org/10.1002/2013JB010803

Husen, S., Taylor, R., Smith, R. B., & Heasler, H. (2004). Changes in geyser eruption behavior and remotely triggered seismicity in Yellowstone National Park produced by the 2002 M 7.9 Denali fault earthquake, Alaska. *Geology*, *32*(6), 537–540. https://doi.org/10.1130/G20381.1

Jaworowski, C., Heasler, H., Neale, C., Saravanan, S., & Masih, A. (2013). Temporal and seasonal variations of the Hot Spring Basin hydrothermal system, Yellowstone National Park, USA. *Remote Sensing*, *5*(12), 6587–6610. https://doi.org/10.3390/rs5126587

Johnson, R. G., & U.S. National Park Service. (1962–1963). Thermal feature images—Geysers—Norris Geyser Basin (images 05161 and 05162), Yellowstone digital slide file. [Photographs of Steamboat Geyser] Retrieved from https://www.nps.gov/features/yell/slidefile/thermalfeatures/geysers/norris/Page.htm

Karlstrom, L., Hurwitz, S., Sohn, R., Vandemeulebrouck, J., Murphy, F., Rudolph, M. L., et al. (2013). Eruptions at lone star geyser, Yellowstone National Park, USA: 1. Energetics and eruption dynamics. *Journal of Geophysical Research: Solid Earth*, *118*(8), 4048–4062. https://doi.org/10.1002/jgrb.50251

Kedar, S., Kanamori, H., & Sturtevant, B. (1998). Bubble collapse as the source of tremor at Old Faithful Geyser. *Journal of Geophysical Research*, *103*(B10), 24283–24299. https://doi.org/10.1029/98JB01824

King, J. (2023). Tree-ring measurement file: Lodgepole pine samples collected at Steamboat Geyser, Yellowstone National Park (decade format (Tucson format, 0.001 mm) text file) [Dataset]. Zenodo. https://doi.org/10.5281/zenodo.8010646

King, J. C. (2014). *NOAA/WDS paleoclimatology—King—Norris upland—PICO—ITRDB WY051*. NOAA National Centers for Environmental Information. https://doi.org/10.25921/421e-4c71

King, J. C. (2016). *Chinese Garden 2016 expanded, Montana-ITRDB-MT153*. National Centers for Environmental Information (NCEI), National Oceanic and Atmospheric Association (NOAA). Retrieved from www.ncdc.noaa.gov/paleo/study/27534

Kiryukhin, A. (2016). Modeling and observations of geyser activity in relation to catastrophic landslides–mudflows (Kronotsky nature reserve, Kamchatka, Russia). *Journal of Volcanology and Geothermal Research*, *323*, 129–147. https://doi.org/10.1016/j.jvolgeores.2016.05.008

Lewicki, J. L., Hilley, G. E., Shelly, D. R., King, J. C., McGeehin, J. P., Mangan, M., & Evans, W. C. (2014). Crustal migration of CO_2-rich magmatic fluids recorded by tree-ring radiocarbon and seismicity at Mammoth Mountain, CA, USA. *Earth and Planetary Science Letters*, *390*, 52–58. https://doi.org/10.1016/j.epsl.2013.12.035

Liesegang, M., & Gee, C. T. (2020). Silica entry and accumulation in standing trees in a hot-spring environment: Cellular pathways, rapid pace and fossilization potential. *Palaeontology*, *63*(4), 651–660. https://doi.org/10.1111/pala.12480

Loader, N. J., Robertson, I., & McCarroll, D. (2003). Comparison of stable carbon isotope ratios in the whole wood, cellulose and lignin of oak tree-rings. *Palaeogeography, Palaeoclimatology, Palaeoecology*, *196*(3–4), 395–407. https://doi.org/10.1016/S0031-0182(03)00466-8

Martin, J. T., Pederson, G. T., Woodhouse, C. A., Cook, E. R., McCabe, G. J., Anchukaitis, K. J., et al. (2020). Increased drought severity tracks warming in the United States' largest river basin. *Proceedings of the National Academy of Sciences of the United States of America*, *117*(21), 11328–11336. https://doi.org/10.1073/pnas.1916208117

Martin, J. T., Pederson, G. T., Woodhouse, C. A., Cook, E. R., McCabe, G. J., Wise, E. K., et al. (2019a). 1200 years of Upper Missouri River streamflow reconstructed from tree rings. *Quaternary Science Reviews*, *224*, 105971. https://doi.org/10.1016/j.quascirev.2019.105971

Martin, J. T., Pederson, G. T., Woodhouse, C. A., Cook, E. R., McCabe, G. J., Wise, E. K., et al. (2019b). A network of 31 Upper Missouri River Basin naturalized water-year (Oct–Sep) streamflow reconstructions spanning years 800–1998 CE. *U.S. Geological Survey Data Release*. https://doi.org/10.5066/P9FC7ILX

Matthews, N. E., Vazquez, J. A., & Calvert, A. T. (2015). Age of the Lava Creek supereruption and magma chamber assembly at Yellowstone based on $^{40}Ar/^{39}Ar$ and U-Pb dating of sanidine and zircon crystals. *Geochemistry, Geophysics, Geosystems*, *16*(8), 2508–2528. https://doi.org/10.1002/2015GC005881

Millspaugh, S. H., & Whitlock, C. (1995). A 750-year fire history based on lake sediment records in central Yellowstone National Park, USA. *The Holocene*, *5*(3), 283–292. https://doi.org/10.1177/095968369500500303

Morgan, L. A., Shanks, W. C. P., Pierce, K. L., Iverson, N., Schiller, C. M., Brown, S. R., et al. (2022). The dynamic floor of Yellowstone Lake, Wyoming, USA: The last 14 ky of hydrothermal explosions, venting, doming, and faulting. *Geological Society of America Bulletin*, *135*(3–4), 547–574. https://doi.org/10.1130/B36190.1

Munoz-Saez, C., Manga, M., Hurwitz, S., Slagter, S., Churchill, D. M., Reich, M., et al. (2020). Radiocarbon dating of silica sinter and postglacial hydrothermal activity in the El Tatio geyser field. *Geophysical Research Letters*, *47*(11), e2020GL087908. https://doi.org/10.1029/2020GL087908

Mustoe, G. E. (2017). Wood petrifaction: A new view of permineralization and replacement. *Geosciences*, *7*(4), 119. https://doi.org/10.3390/geosciences7040119

Nayak, A., Manga, M., Hurwitz, S., Namiki, A., & Dawson, P. B. (2020). Origin and properties of hydrothermal tremor at Lone Star Geyser, Yellowstone National Park, USA. *Journal of Geophysical Research: Solid Earth*, *125*(12), e2020JB019711. https://doi.org/10.1029/2020JB019711

Peale, A. C. (1883). Some geyser comparisons. *Science*, (25), 101–102. https://doi.org/10.1126/science.ns-2.25.101

Pederson, G. T., Betancourt, J. L., & McCabe, G. J. (2013). Regional patterns and proximal causes of the recent snowpack decline in the Rocky Mountains, US. *Geophysical Research Letters*, *40*(9), 1811–1816. https://doi.org/10.1002/grl.50424

Pederson, G. T., Gray, S. T., Woodhouse, C. A., Betancourt, J. L., Fagre, D. B., Littell, J. S., et al. (2011). The unusual nature of recent snowpack declines in the North American Cordillera. *Science*, *333*(6040), 332–335. https://doi.org/10.1126/science.1201570

Pierce, K. L., Cannon, K. P., Meyer, G. A., Trebesch, M. J., & Watts, R. D. (2002). Post-glacial inflation-deflation cycles, tilting, and faulting in the Yellowstone caldera based on Yellowstone Lake shorelines. *US Geological Survey Open-File Report*, *142*, 30. http://pubs.usgs.gov/of/2002/ofr-02-0142/

R Development Core Team. (2022). *R: A language and environment for statistical computing*. R Foundation for Statistical Computing. Retrieved from https://www.r-project.org/

Reed, M. H., Munoz-Saez, C., Hajimirza, S., Wu, S. M., Barth, A., Girona, T., et al. (2021). The 2018 reawakening and eruption dynamics of Steamboat Geyser, the world's tallest active geyser. *Proceedings of the National Academy of Sciences of the United States of America*, *118*(2), e2020943118. https://doi.org/10.1073/pnas.2020943118

Reimer, P. J., Austin, W. E., Bard, E., Bayliss, A., Blackwell, P. G., Ramsey, C. B., et al. (2020). The IntCal20 Northern Hemisphere radiocarbon age calibration curve (0–55 cal kBP). *Radiocarbon*, *62*(4), 725–757. https://doi.org/10.1017/RDC.2020.41

Schiller, C. M., Whitlock, C., Alt, M., & Morgan, L. A. (2020). Vegetation responses to quaternary volcanic and hydrothermal disturbances in the northern Rocky Mountains and greater Yellowstone ecosystem (USA). *Palaeogeography, Palaeoclimatology, Palaeoecology*, *559*, 109859. https://doi.org/10.1016/j.palaeo.2020.109859

Schiller, C. M., Whitlock, C., & Brown, S. R. (2022). Holocene geo-ecological evolution of Lower Geyser Basin, Yellowstone National Park (USA). *Quaternary Research*, *105*, 201–217. https://doi.org/10.1017/qua.2021.42

Schiller, C. M., Whitlock, C., Elder, K. L., Iverson, N. A., & Abbott, M. B. (2021). Erroneously old radiocarbon ages from terrestrial pollen concentrates in Yellowstone Lake, Wyoming, USA. *Radiocarbon*, *63*(1), 321–342. https://doi.org/10.1017/RDC.2020.118

Schroeder, R. K. (1963). *Steamboat Geyser eruption heights. Geology program records (Box 120)*. Yellowstone National Park Archives.

Shean, D. (2006). Norris Geyser Basin's dynamic hydrothermal features: Using historical aerial photographs to detect change. *Yellowstone Science*, *14*, 24–28.

Shuman, B. N., & Serravezza, M. (2017). Patterns of hydroclimatic change in the Rocky Mountains and surrounding regions since the last glacial maximum. *Quaternary Science Reviews*, *173*, 58–77. https://doi.org/10.1016/j.quascirev.2017.08.01

Slagter, S., Reich, M., Munoz-Saez, C., Southon, J., Morata, D., Barra, F., et al. (2019). Environmental controls on silica sinter formation revealed by radiocarbon dating. *Geology*, *47*(4), 330–334. https://doi.org/10.1130/g45859.1

Stokes, M. A., & Smiley, T. L. (1968). *An introduction to tree-ring dating*. University of Chicago Press.

Swetnam, T. W., Thompson, M. A., & Sutherland, E. K. (1985). *Using dendrochronology to measure radial growth of defoliated trees*. US Department of Agriculture, Forest Service, Cooperative State Research Service.

Turner, M. G., Braziunas, K. H., Hansen, W. D., Hoecker, T. J., Rammer, W., Ratajczak, Z., et al. (2022). The magnitude, direction, and tempo of forest change in Greater Yellowstone in a warmer world with more fire. *Ecological Monographs*, *92*(1), e01485. https://esajournals.onlinelibrary.wiley.com/doi/full/10.1002/ecm.1485

U.S. Geological Survey. (2022). National water information system [Dataset]. U.S. Geological Survey Web Interface. Retrieved from https://nwis.waterdata.usgs.gov/nwis

Vandemeulebrouck, J., Sohn, R. A., Rudolph, M. L., Hurwitz, S., Manga, M., Johnston, M. J., et al. (2014). Eruptions at lone star geyser, Yellowstone National Park, USA: 2. Constraints on subsurface dynamics. *Journal of Geophysical Research: Solid Earth*, *119*(12), 8688–8707. https://doi.org/10.1002/2014JB011526

White, D. E., (1992). The Beowawe Geysers, Nevada, before geothermal development. *U.S. Geological Survey Bulletin, 1998*, 25. https://doi.org/10.3133/b1998

White, D. E., Keith, T. E., & Hutchinson, R. A. (1988). The geology and remarkable thermal activity of Norris Geyser basin, Yellowstone National Park, Wyoming. U.S. Geological Survey Professional Paper 1456. https://doi.org/10.3133/pp1456

Whitlock, C., Dean, W. E., Fritz, S. C., Stevens, L. R., Stone, J. R., Power, M. J., et al. (2012). Holocene seasonal variability inferred from multiple proxy records from Crevice Lake, Yellowstone National Park, USA. *Palaeogeography, Palaeoclimatology, Palaeoecology*, *331*, 90–103. https://doi.org/10.1016/j.palaeo.2012.03.001

Whittlesey, L. H., & Watry, E. A. (2008). *Yellowstone National Park* (p. 128). Arcadia Publishing.

Wicks, C. W., Dzurisin, D., Lowenstern, J. B., & Svarc, J. (2020). Magma intrusion and volatile ascent beneath Norris Geyser basin, Yellowstone National Park. *Journal of Geophysical Research: Solid Earth*, *125*(2), e2019JB018208. https://doi.org/10.1029/2019JB018208

Williams, A. P., Cook, E. R., Smerdon, J. E., Cook, B. I., Abatzoglou, J. T., Bolles, K., et al. (2020). Large contribution from anthropogenic warming to an emerging North American megadrought. *Science*, *368*(6488), 314–318. https://doi.org/10.1126/science.aaz9600

Wu, S. M., Lin, F. C., Farrell, J., & Allam, A. (2019). Imaging the deep subsurface plumbing of Old Faithful geyser from low-frequency hydrothermal tremor migration. *Geophysical Research Letters*, *46*(13), 7315–7322. https://doi.org/10.1029/2018GL081771

Wu, S. M., Lin, F. C., Farrell, J., Keller, W. E., White, E. B., & Hungerford, J. D. (2021). Imaging the subsurface plumbing complex of Steamboat Geyser and Cistern Spring with hydrothermal tremor migration using seismic interferometry. *Journal of Geophysical Research: Solid Earth*, *126*(4), e2020JB021128. https://doi.org/10.1029/2020JB021128